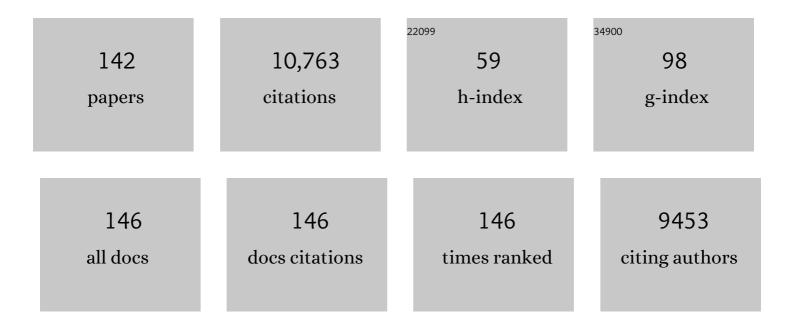
## Afonso C Silva

List of Publications by Year in descending order

Source: https://exaly.com/author-pdf/5317907/publications.pdf Version: 2024-02-01



#	Article	IF	CITATIONS
1	Manganese-enhanced magnetic resonance imaging (MEMRI): methodological and practical considerations. NMR in Biomedicine, 2004, 17, 532-543.	1.6	457
2	In vivo neuronal tract tracing using manganese-enhanced magnetic resonance imaging. Magnetic Resonance in Medicine, 1998, 40, 740-748.	1.9	434
3	Highly efficient endosomal labeling of progenitor and stem cells with large magnetic particles allows magnetic resonance imaging of single cells. Blood, 2003, 102, 867-872.	0.6	404
4	Superficial white matter fiber systems impede detection of long-range cortical connections in diffusion MR tractography. Proceedings of the National Academy of Sciences of the United States of America, 2015, 112, E2820-8.	3.3	364
5	Tissue specific perfusion imaging using arterial spin labeling. NMR in Biomedicine, 1994, 7, 75-82.	1.6	301
6	Diffusion-weighted spin-echo fMRI at 9.4 T: Microvascular/tissue contribution to BOLD signal changes. Magnetic Resonance in Medicine, 1999, 42, 919-928.	1.9	279
7	Marmosets: A Neuroscientific Model of Human Social Behavior. Neuron, 2016, 90, 219-233.	3.8	260
8	In vivo detection of neuroarchitecture in the rodent brain using manganese-enhanced MRI. NeuroImage, 2004, 22, 1046-1059.	2.1	246
9	Laminar specificity of functional MRI onset times during somatosensory stimulation in rat. Proceedings of the National Academy of Sciences of the United States of America, 2002, 99, 15182-15187.	3.3	244
10	Functional MRI of calcium-dependent synaptic activity: Cross correlation with CBF and BOLD measurements. Magnetic Resonance in Medicine, 2000, 43, 383-392.	1.9	242
11	Sensitivity of MRI resonance frequency to the orientation of brain tissue microstructure. Proceedings of the National Academy of Sciences of the United States of America, 2010, 107, 5130-5135.	3.3	238
12	Brains, Genes, and Primates. Neuron, 2015, 86, 617-631.	3.8	231
13	Simultaneous Blood Oxygenation Level-Dependent and Cerebral Blood Flow Functional Magnetic Resonance Imaging during Forepaw Stimulation in the Rat. Journal of Cerebral Blood Flow and Metabolism, 1999, 19, 871-879.	2.4	230
14	Manganese-enhanced magnetic resonance imaging (MEMRI). NMR in Biomedicine, 2004, 17, 527-531.	1.6	217
15	Functional Reactivity of Cerebral Capillaries. Journal of Cerebral Blood Flow and Metabolism, 2008, 28, 961-972.	2.4	189
16	The contribution of myelin to magnetic susceptibility-weighted contrasts in high-field MRI of the brain. NeuroImage, 2012, 59, 3967-3975.	2.1	186
17	Micro-compartment specific T2â $\check{ extsf{Z}}$ relaxation in the brain. NeuroImage, 2013, 77, 268-278.	2.1	182
18	Manganese-Enhanced MRI: An Exceptional Tool in Translational Neuroimaging. Schizophrenia Bulletin, 2007, 34, 595-604.	2.3	162

#	Article	IF	CITATIONS
19	Early Temporal Characteristics of Cerebral Blood Flow and Deoxyhemoglobin Changes during Somatosensory Stimulation. Journal of Cerebral Blood Flow and Metabolism, 2000, 20, 201-206.	2.4	157
20	Manganese-enhanced magnetic resonance imaging of mouse brain after systemic administration of MnCl2: Dose-dependent and temporal evolution ofT1 contrast. Magnetic Resonance in Medicine, 2005, 53, 640-648.	1.9	154
21	Multi-Slice MRI of Rat Brain Perfusion During Amphetamine Stimulation Using Arterial Spin Labeling. Magnetic Resonance in Medicine, 1995, 33, 209-214.	1.9	149
22	NMR Measurement of Perfusion Using Arterial Spin Labeling Without Saturation of Macromolecular Spins. Magnetic Resonance in Medicine, 1995, 33, 370-376.	1.9	147
23	Functional Mapping of Face-Selective Regions in the Extrastriate Visual Cortex of the Marmoset. Journal of Neuroscience, 2015, 35, 1160-1172.	1.7	137
24	Large-Scale Brain Networks in the Awake, Truly Resting Marmoset Monkey. Journal of Neuroscience, 2013, 33, 16796-16804.	1.7	133
25	Visualizing the entire cortical myelination pattern in marmosets with magnetic resonance imaging. Journal of Neuroscience Methods, 2009, 185, 15-22.	1.3	127
26	A digital 3D atlas of the marmoset brain based on multi-modal MRI. NeuroImage, 2018, 169, 106-116.	2.1	127
27	Dynamic activity-induced manganese-dependent contrast magnetic resonance imaging (DAIM MRI). Magnetic Resonance in Medicine, 2002, 48, 927-933.	1.9	126
28	Functional MRI impulse response for BOLD and CBV contrast in rat somatosensory cortex. Magnetic Resonance in Medicine, 2007, 57, 1110-1118.	1.9	126
29	Spatial flow-volume dissociation of the cerebral microcirculatory response to mild hypercapnia. NeuroImage, 2006, 32, 520-530.	2.1	118
30	T 2 *-based fiber orientation mapping. NeuroImage, 2011, 57, 225-234.	2.1	118
31	Temporal dynamics of the BOLD fMRI impulse response. NeuroImage, 2005, 24, 667-677.	2.1	110
32	Imaging blood flow in brain tumors using arterial spin labeling. Magnetic Resonance in Medicine, 2000, 44, 169-173.	1.9	109
33	Spatiotemporal Evolution of the Functional Magnetic Resonance Imaging Response to Ultrashort Stimuli. Journal of Neuroscience, 2011, 31, 1440-1447.	1.7	104
34	Estimation of water extraction fractions in rat brain using magnetic resonance measurement of perfusion with arterial spin labeling. Magnetic Resonance in Medicine, 1997, 37, 58-68.	1.9	102
35	Sensory and optogenetically driven single-vessel fMRI. Nature Methods, 2016, 13, 337-340.	9.0	98
36	Functional MRI of the rodent somatosensory pathway using multislice echo planar imaging. Magnetic Resonance in Medicine, 2004, 52, 89-99.	1.9	97

#	Article	IF	CITATIONS
37	Evidence for the exchange of arterial spin-labeled water with tissue water in rat brain from diffusion-sensitized measurements of perfusion. Magnetic Resonance in Medicine, 1997, 38, 232-237.	1.9	92
38	Direct magnetic resonance detection of neuronal electrical activity. Proceedings of the National Academy of Sciences of the United States of America, 2006, 103, 16015-16020.	3.3	92
39	Accelerating the Evolution of Nonhuman Primate Neuroimaging. Neuron, 2020, 105, 600-603.	3.8	92
40	Direct imaging of macrovascular and microvascular contributions to BOLD fMRI in layers IV–V of the rat whisker–barrel cortex. NeuroImage, 2012, 59, 1451-1460.	2.1	89
41	The formation of inflammatory demyelinated lesions in cerebral white matter. Annals of Neurology, 2014, 76, 594-608.	2.8	89
42	fMRI in the awake marmoset: Somatosensory-evoked responses, functional connectivity, and comparison with propofol anesthesia. NeuroImage, 2013, 78, 186-195.	2.1	87
43	Glutamate neurons are intermixed with midbrain dopamine neurons in nonhuman primates and humans. Scientific Reports, 2016, 6, 30615.	1.6	84
44	Pseudo-continuous arterial spin labeling technique for measuring CBF dynamics with high temporal resolution. Magnetic Resonance in Medicine, 1999, 42, 425-429.	1.9	83
45	Anatomical and functional investigation of the marmoset default mode network. Nature Communications, 2019, 10, 1975.	5.8	82
46	Generation of transgenic marmosets expressing genetically encoded calcium indicators. Scientific Reports, 2016, 6, 34931.	1.6	81
47	Fractionated manganeseâ€enhanced MRI. NMR in Biomedicine, 2008, 21, 473-478.	1.6	79
48	Elevated endogenous GABA level correlates with decreased fMRI signals in the rat brain during acute inhibition of GABA transaminase. Journal of Neuroscience Research, 2005, 79, 383-391.	1.3	78
49	A combined histological and MRI brain atlas of the common marmoset monkey, Callithrix jacchus. Brain Research Reviews, 2009, 62, 1-18.	9.1	78
50	Cell labeling for magnetic resonance imaging with theT1 agent manganese chloride. NMR in Biomedicine, 2006, 19, 50-59.	1.6	77
51	A resource for the detailed 3D mapping of white matter pathways in the marmoset brain. Nature Neuroscience, 2020, 23, 271-280.	7.1	77
52	BOLD and CBV-weighted functional magnetic resonance imaging of the rat somatosensory system. Magnetic Resonance in Medicine, 2006, 55, 316-324.	1.9	76
53	Longitudinal Functional Magnetic Resonance Imaging in Animal Models. Methods in Molecular Biology, 2011, 711, 281-302.	0.4	76
54	Detection of cortical laminar architecture using manganese-enhanced MRI. Journal of Neuroscience Methods, 2008, 167, 246-257.	1.3	72

#	Article	IF	CITATIONS
55	Cerebrospinal fluid to brain transport of manganese in a non-human primate revealed by MRI. Brain Research, 2008, 1198, 160-170.	1.1	72
56	Functional Uncoupling of Hemodynamic from Neuronal Response by Inhibition of Neuronal Nitric Oxide Synthase. Journal of Cerebral Blood Flow and Metabolism, 2007, 27, 741-754.	2.4	71
57	In vivo quantification of T2⎠anisotropy in white matter fibers in marmoset monkeys. NeuroImage, 2012, 59, 979-985.	2.1	70
58	Perfusion imaging using dynamic arterial spin labeling (DASL). Magnetic Resonance in Medicine, 2001, 45, 1021-1029.	1.9	69
59	Differential Effects of NMDA and AMPA Glutamate Receptors on Functional Magnetic Resonance Imaging Signals and Evoked Neuronal Activity during Forepaw Stimulation of the Rat. Journal of Neuroscience, 2006, 26, 8409-8416.	1.7	66
60	Comparison of diffusion-weighted high-resolution CBF and spin-echo BOLD fMRI at 9.4 T. Magnetic Resonance in Medicine, 2002, 47, 736-741.	1.9	62
61	Manganese enhanced MRI reveals functional circuitry in response to odorant stimuliâ~†. NeuroImage, 2009, 44, 363-372.	2.1	61
62	Cyclooxygenase-1 and -2 Differentially Modulate Lipopolysaccharide-Induced Blood–Brain Barrier Disruption through Matrix Metalloproteinase Activity. Journal of Cerebral Blood Flow and Metabolism, 2010, 30, 370-380.	2.4	61
63	On the contribution of deoxy-hemoglobin to MRI gray–white matter phase contrast at high field. NeuroImage, 2010, 49, 193-198.	2.1	61
64	Functional MRI of visual responses in the awake, behaving marmoset. NeuroImage, 2015, 120, 1-11.	2.1	61
65	MRI detection of ferritin iron overload and associated neuronal pathology in iron regulatory protein-2 knockout mice. Brain Research, 2003, 971, 95-106.	1.1	57
66	Modulatory role of cyclooxygenase-2 in cerebrovascular coupling. NeuroImage, 2006, 32, 23-32.	2.1	54
67	Marmoset Brain Mapping V3: Population multi-modal standard volumetric and surface-based templates. NeuroImage, 2021, 226, 117620.	2.1	50
68	Spatiotemporal distribution of fibrinogen in marmoset and human inflammatory demyelination. Brain, 2018, 141, 1637-1649.	3.7	49
69	Measurement of cerebral perfusion territories using arterial spin labelling. NMR in Biomedicine, 2007, 20, 633-642.	1.6	48
70	Magnetic resonance imaging quantification of regional cerebral blood flow and cerebrovascular reactivity to carbon dioxide in normotensive and hypertensive rats. NeuroImage, 2011, 58, 75-81.	2.1	47
71	Novel Marmoset (Callithrix jacchus) Model of Human Herpesvirus 6A and 6B Infections: Immunologic, Virologic and Radiologic Characterization. PLoS Pathogens, 2013, 9, e1003138.	2.1	47
72	Layer specific tracing of corticocortical and thalamocortical connectivity in the rodent using manganese enhanced MRI. NeuroImage, 2009, 44, 923-931.	2.1	45

#	Article	IF	CITATIONS
73	Potential role of iron in repair of inflammatory demyelinating lesions. Journal of Clinical Investigation, 2019, 129, 4365-4376.	3.9	45
74	Perfusion analysis using dynamic arterial spin labeling (DASL). Magnetic Resonance in Medicine, 1999, 41, 299-308.	1.9	42
75	Herpesvirus trigger accelerates neuroinflammation in a nonhuman primate model of multiple sclerosis. Proceedings of the National Academy of Sciences of the United States of America, 2018, 115, 11292-11297.	3.3	40
76	Two-photon imaging of cerebral hemodynamics and neural activity in awake and anesthetized marmosets. Journal of Neuroscience Methods, 2016, 271, 55-64.	1.3	38
77	The role of nitrite in neurovascular coupling. Brain Research, 2011, 1407, 62-68.	1.1	37
78	Visualizing myeloarchitecture with magnetic resonance imaging in primates. Annals of the New York Academy of Sciences, 2011, 1225, E171-81.	1.8	35
79	An embedded fourâ€channel receiveâ€only RF coil array for fMRI experiments of the somatosensory pathway in conscious awake marmosets. NMR in Biomedicine, 2013, 26, 1395-1402.	1.6	35
80	Anatomical and functional neuroimaging in awake, behaving marmosets. Developmental Neurobiology, 2017, 77, 373-389.	1.5	35
81	Generation of genetically engineered nonâ€human primate models of brain function and neurological disorders. American Journal of Primatology, 2019, 81, e22931.	0.8	34
82	Neuroprotective Effects of MAGL (Monoacylglycerol Lipase) Inhibitors in Experimental Ischemic Stroke. Stroke, 2018, 49, 718-726.	1.0	31
83	BOLD fMRI and somatosensory evoked potentials are well correlated over a broad range of frequency content of somatosensory stimulation of the rat forepaw. Brain Research, 2008, 1195, 67-76.	1.1	28
84	In vivo visualization of reactive gliosis using manganese-enhanced magnetic resonance imaging. NeuroImage, 2010, 49, 3122-3131.	2.1	28
85	Rapid high-resolution three-dimensional mapping of T1 and age-dependent variations in the non-human primate brain using magnetization-prepared rapid gradient-echo (MPRACE) sequence. NeuroImage, 2011, 56, 1154-1163.	2.1	27
86	Perivenular brain lesions in a primate multiple sclerosis model at 7-tesla magnetic resonance imaging. Multiple Sclerosis Journal, 2014, 20, 64-71.	1.4	25
87	Histologyâ€Based Average Template of the Marmoset Cortex With Probabilistic Localization of Cytoarchitectural Areas. NeuroImage, 2021, 226, 117625.	2.1	25
88	Manganeseâ€enhanced MRI visualizes V1 in the nonâ€human primate visual cortex. NMR in Biomedicine, 2009, 22, 730-736.	1.6	24
89	The Stability of the Blood Oxygenation Level-Dependent Functional MRI Response to Motor Tasks Is Altered in Patients With Chronic Ischemic Stroke. Stroke, 2010, 41, 1921-1926.	1.0	24
90	Assessing Cerebrovascular Reactivity in Carotid Steno-Occlusive Disease Using MRI BOLD and ASL Techniques. Radiology Research and Practice, 2012, 2012, 1-10.	0.6	24

#	Article	IF	CITATIONS
91	Custom fit 3D-printed brain holders for comparison of histology with MRI in marmosets. Journal of Neuroscience Methods, 2016, 257, 55-63.	1.3	24
92	Manganeseâ€enhanced magnetic resonance imaging detects mossy fiber sprouting in the pilocarpine model of epilepsy. Epilepsia, 2012, 53, 1225-1232.	2.6	23
93	Utilizing 3D Printing Technology to Merge MRI with Histology: A Protocol for Brain Sectioning. Journal of Visualized Experiments, 2016, , .	0.2	23
94	An open access resource for functional brain connectivity from fully awake marmosets. NeuroImage, 2022, 252, 119030.	2.1	23
95	Functional Connectivity Hubs and Networks in the Awake Marmoset Brain. Frontiers in Integrative Neuroscience, 2016, 10, 9.	1.0	22
96	Toward next-generation primate neuroscience: A collaboration-based strategic plan for integrative neuroimaging. Neuron, 2022, 110, 16-20.	3.8	22
97	Using manganese-enhanced MRI to understand BOLD. NeuroImage, 2012, 62, 1009-1013.	2.1	21
98	Functional magnetic resonance imaging of auditory cortical fields in awake marmosets. Neurolmage, 2017, 162, 86-92.	2.1	21
99	Manganese-enhanced magnetic resonance imaging (MEMRI) of rat brain after systemic administration of MnCl2: Changes in T1 relaxation times during postnatal development. Journal of Magnetic Resonance Imaging, 2007, 25, 32-38.	1.9	20
100	Investigating the spatiotemporal characteristics of the deoxyhemoglobin-related and deoxyhemoglobin-unrelated functional hemodynamic response across cortical layers in awake marmosets. Neurolmage, 2018, 164, 121-130.	2.1	20
101	Hardware considerations for functional magnetic resonance imaging. Concepts in Magnetic Resonance, 2003, 16A, 35-49.	1.3	19
102	Design and implementation of embedded 8 hannel receiveâ€only arrays for wholeâ€brain MRI and fMRI of conscious awake marmosets. Magnetic Resonance in Medicine, 2017, 78, 387-398.	1.9	18
103	Investigation of the BOLD and CBV fMRI responses to somatosensory stimulation in awake marmosets ( <scp><i>Callithrix jacchus</i></scp> ). NMR in Biomedicine, 2018, 31, e3864.	1.6	18
104	Perfusion-based functional magnetic resonance imaging. Concepts in Magnetic Resonance, 2003, 16A, 16-27.	1.3	17
105	Traits of fear resistance and susceptibility in an advanced intercross line. European Journal of Neuroscience, 2013, 38, 3314-3324.	1.2	17
106	Impaired CBF regulation and high CBF threshold contribute to the increased sensitivity of spontaneously hypertensive rats to cerebral ischemia. Neuroscience, 2014, 269, 223-231.	1.1	17
107	Cannabis and Cannabinoid Biology in Stroke. Stroke, 2019, 50, 2640-2645.	1.0	17
108	Radial Echo-Planar Imaging. Journal of Magnetic Resonance, 1998, 135, 242-247.	1.2	16

#	Article	IF	CITATIONS
109	Manganese: a unique neuroimaging contrast agent. Future Neurology, 2007, 2, 297-305.	0.9	16
110	Simultaneous Glutamate and Perfusion fMRI Responses to Regional Brain Stimulation. Journal of Cerebral Blood Flow and Metabolism, 1998, 18, 1064-1070.	2.4	15
111	Spatial organization of occipital white matter tracts in the common marmoset. Brain Structure and Function, 2020, 225, 1313-1326.	1.2	14
112	Using non-invasive neuroimaging to enhance the care, well-being and experimental outcomes of laboratory non-human primates (monkeys). NeuroImage, 2021, 228, 117667.	2.1	13
113	Arterial spin labeling of cerebral perfusion territories using a separate labeling coil. Journal of Magnetic Resonance Imaging, 2008, 27, 970-977.	1.9	12
114	Perfusion-based fMRI: Insights from animal models. Journal of Magnetic Resonance Imaging, 2005, 22, 745-750.	1.9	11
115	Highâ€field continuous arterial spin labeling with long labeling duration: Reduced confounds from blood transit time and postlabeling delay. Magnetic Resonance in Medicine, 2010, 64, 1557-1566.	1.9	10
116	Phenylephrine-induced hypertension during transient middle cerebral artery occlusion alleviates ischemic brain injury in spontaneously hypertensive rats. Brain Research, 2012, 1477, 83-91.	1.1	10
117	Direct Interhemispheric Cortical Communication via Thalamic Commissures: A New White-Matter Pathway in the Rodent Brain. Cerebral Cortex, 2021, 31, 4642-4651.	1.6	9
118	The spectrum of spinal cord lesions in a primate model of multiple sclerosis. Multiple Sclerosis Journal, 2020, 26, 284-293.	1.4	8
119	Long-distance aberrant heterotopic connectivity in a mouse strain with a high incidence of callosal anomalies. Neurolmage, 2020, 217, 116875.	2.1	8
120	Magnetic Resonance Imaging of Marmoset Monkeys. ILAR Journal, 2020, 61, 274-285.	1.8	8
121	Corpus callosum dysgenesis causes novel patterns of structural and functional brain connectivity. Brain Communications, 2021, 3, fcab057.	1.5	8
122	Arterial Spin Labeling Measurements of Cerebral Perfusion Territories in Experimental Ischemic Stroke. Translational Stroke Research, 2012, 3, 44-55.	2.3	7
123	Ultrahigh-resolution MRI Reveals Extensive Cortical Demyelination in a Nonhuman Primate Model of Multiple Sclerosis. Cerebral Cortex, 2021, 31, 439-447.	1.6	7
124	Dynamic Magnetic Resonance Imaging of Cerebral Blood Flow Using Arterial Spin Labeling. Methods in Molecular Biology, 2009, 489, 277-295.	0.4	5
125	Dynamic Interhemispheric Desynchronization in Marmosets and Humans With Disorders of the Corpus Callosum. Frontiers in Neural Circuits, 2020, 14, 612595.	1.4	4
126	The Brain Circuits and Dynamics of Curiosity-Driven Behavior in Naturally Curious Marmosets. Cerebral Cortex, 2021, 31, 4220-4232.	1.6	4

#	Article	IF	CITATIONS
127	Arterial spin labeling demonstrates that focal amygdalar glutamatergic agonist infusion leads to rapid diffuse cerebral activation. Acta Neurologica Scandinavica, 2010, 121, 209-216.	1.0	3
128	Pseudo-continuous arterial spin labeling technique for measuring CBF dynamics with high temporal resolution. , 1999, 42, 425.		3
129	An open transversez-gradient coil design for magnetic resonance imaging. Review of Scientific Instruments, 2002, 73, 2208-2210.	0.6	2
130	Rapid BOLD Attenuation in Stroke Patients Detected by a Parametric Analysis. NeuroImage, 2009, 47, S94.	2.1	2
131	Diffusion-weighted spin-echo fMRI at 9.4 T: Microvascular/tissue contribution to BOLD signal changes. , 1999, 42, 919.		2
132	In vivo detection of neuroarchitecture in the rodent brain using manganese-enhanced MRI. NeuroImage, 2004, 22, 1046-1046.	2.1	1
133	Manganese-Enhanced Magnetic Resonance Imaging: Applications to Preclinical Research*. , 2010, , 199-219.		1
134	Quantification of BOLD fMRI parameters to infer cerebrovascular reactivity of the middle cerebral artery. Journal of Magnetic Resonance Imaging, 2013, 38, 1203-1209.	1.9	1
135	Contrast Agents in Functional Magnetic Resonance Imaging. , 2015, , 37-46.		1
136	Perfusion analysis using dynamic arterial spin labeling (DASL). , 1999, 41, 299.		1
137	MRI detection of regional blood flow using arterial spin labeling. , 2004, , 119-140.		Ο
138	Detection of regional blood flow using arterial spin labeling. , 0, , 94-112.		0
139	NO Production in Rat Brain – Possible Nonenzymatic Pathways. Free Radical Biology and Medicine, 2012, 53, S185.	1.3	0
140	Visualizing Myeloarchitecture In Vivo with Magnetic Resonance Imaging in Common Marmosets (Callithrix jacchus). , 2013, , 221-237.		0
141	Animal Models in Functional Magnetic Resonance Imaging. , 2008, , 483-498.		Ο
142	Current Topics in Research, Care, and Welfare of Common Marmosets. ILAR Journal, 0, , .	1.8	0